Supplement of

Distinct Spatiotemporal Patterns of Atmospheric Total and Soluble Iron from Three Sources Revealed by Shipboard Online Observations in the Northwest Pacific

5 Tianle Zhang et al.

Correspondence to: Mei Zheng (mzheng@pku.edu.cn)
The copyright of individual parts of the supplement might differ from the article licence.

Text S1. Analytic procedure for filter samples

10

20

40

For total elements digestion, an entire PTFE filter (46.2 mm diameter, Whatman) was cut into fragments and placed in a PTFE digestion jar. Prior to use, all digestion jars were rigorously cleaned with deionized water, hydrochloric acid (HCl), and nitric acid (HNO₃), following the procedure described in Zhang et al. (2022). The filter fragments were first pre-digested at room temperature for 12 hours with 2 mL of HNO₃ (69% w/w) and 2.5 mL of hydrogen peroxide (H₂O₂) (31% w/w), followed by the addition of 3 mL HNO₃ (69% w/w) and 1 mL hydrofluoric acid (HF) for microwave digestion. Digestion was carried out using a microwave digestion system (TOPEX+, PreeKem Co., Ltd.) under a temperature-controlled program: ramp to 50 °C in 5 min and hold for 5 min; ramp to 120 °C in 10 min and hold for 15 min; ramp to 180 °C in 10 min and hold for 30 min; followed by a 20 min cooling phase to 50 °C. After digestion, the jars were transferred to a heating plate and heated at 140 °C to evaporate residual acids to near-dryness. The digestates were then reconstituted to 20 mL with 1% (v/v) HNO₃ and filtered through a 0.22 µm pore-size polyethersulfone (PES) syringe filter.

For soluble element extraction, another entire PTFE filter (46.2 mm diameter, Whatman) was cut into fragments and placed in a centrifuge tube. A 5 mM ammonium acetate-acetic acid buffer solution (pH 4.7) was freshly prepared by dissolving 0.7758 g ammonium acetate and 571 μ L acetic acid in 2 L ultrapure water. Each centrifuge tube containing filter fragments was treated with 10 mL of the buffer solution, sealed tightly, and horizontally shaken (ZWHZ-08A oscillator, 300 rpm) for 2 hours at room temperature. After shaking, the supernatant was filtered through a 0.22 μ m PES syringe filter and collected into pre-labeled centrifuge tubes. Subsequently, 144 μ L of HNO₃ (69% w/w) was added to each tube to obtain a final test solution with a substrate of 1% (v/v) HNO₃.

Elemental concentrations of Al, Fe, Ba, Mn, Cr, Cu, Zn, Pb, V, Ni, As, Se, Cd, and Sb were quantified using inductively coupled plasma mass spectrometry (ICP-MS; iCAP Q, Thermo Fisher Scientific). Four field blanks were analyzed, including two for acid digestion and two for buffer extraction. Elemental concentrations in ambient samples were corrected by subtracting the blank value.

Text S2. Definition and screening method for outliers

Outlier screening was conducted in two steps: automated screening followed by manual verification. The automated screening was performed using custom MATLAB code. In the script, a variable called the "beside-mean" was defined. For instance, the beside-mean of Fe in the 100th sample was calculated as the average concentration of Fe in the 98th, 99th, 101st, and 102nd samples. If the Fe concentration in the 100th sample exceeded 1.8 times or was less than 0.2 times its beside-mean (>1.8×beside-mean or <0.2×beside-mean), it was automatically flagged as an outlier.

The flagged outliers were then subjected to manual review. An outlier was confirmed manually only if it met both of the following criteria: (1) the outlier was temporally discontinuous, with no abnormal concentrations observed in the adjacent samples; and (2) only one element associated with a specific source showed an abnormal concentration in the sample, while other elements associated with the source in this sample remained within normal ranges.

Text S3. Preparation of input data for Positive Matrix Factorization (PMF)

Positive Matrix Factorization requires the input of both measured chemical species concentrations and their associated uncertainties. For concentration data, values below the minimum detection limit (MDL) were replaced with half the MDL.

For uncertainty calculations, two approaches were applied based on the measured concentration relative to the MDL. If the concentration of a species was less than or equal to the MDL, the uncertainty (Unc) was calculated as a fixed fraction of the MDL, as shown in Equation (1). If the concentration exceeded the MDL, the uncertainty was calculated using Equation (2), where the error fraction was set to 0.2.

$$Unc = \frac{5}{6}MDL \tag{1}$$

Unc =
$$\sqrt{(Error\ Fraction \times concentration)^2 + (0.5 \times MDL)^2}$$
 (2)

Text S4. Testing of the PMF model

50

55

60

65

70

The number of factors in the PMF model was selected using two criteria: (1) diagnostic indicators recommended in the PMF operational guidelines, and (2) the allocation of source tracers within each factor (Gary et al., 2014). Using the PM₁₀ samples source apportionment as an example, we varied the number of factors from three to eight to identify the optimum. As the number increased, the ratio of Q_{true} to Q_{robust} remained between 1.2 and 1.6, which indicated limited influence from data points with large residuals. The value of Q relative to Q_{expected} reached its minimum at seven factors, which suggested that the mathematical diagnostics favored a seven-factor solution.

Despite this, closer examination of the seven-factor profiles revealed several factors that were difficult to interpret. Some factors were dominated solely by Se, Ni, or Ca, without other supporting tracers, making it difficult to link them to specific emission sources. In contrast, reducing the model to three factors eliminated these anomalous single element factors, and each factor exhibited a clear association with an identifiable source. Under the three-factor solution, Fe concentrations were reconstructed from the PMF outputs according to Equation (3). The reconstructed Fe concentrations correlated strongly with the measurements, with R² equal to 0.88 and a linear regression slope of 1.14 as shown in Fig. S3a. This result indicated that the three-factor solution provided strong predictive capability for ambient Fe concentrations.

$$PMF_Fe_i = \sum_{j=1}^3 (Fe_j \times R_{i,j})$$
(3)

where PMF_Fe_i represents the PMF-reconstructed Fe concentration in sample i (unit: $ng m^{-3}$); Fe_j denotes the Fe concentration in the profile of factor j (unit: $ng m^{-3}$); R_{ij} indicates the contribution of the factor j to sample i (dimensionless).

We applied the same source analysis approach to Fe in PM_{2.5} samples from the NWP1 cruise. Testing different factor numbers again identified a three-factor solution as optimal. The reconstructed Fe concentrations agreed well with the measured values, with R² equal to 0.85 and a linear regression slope of 1.21 as shown in Fig. S3b.

Table S1. Elemental concentration in marine aerosols over the Chinese marginal Seas and the open Northwest Pacific based on measurements (unit: ng m⁻³)

	This study			Shimada et al. (2018)		Ge et al. (2024)	Zhang et al. (2024)		Jin et al. (2019)
Sea area	BY cruise	NWP1 cruise	NWP2 cruise	Tuoji Island, Bohai Sea	Cape Hedo, East China Sea	Chinese marginal Seas	Yellow Sea and East China Sea	Open Northwest Pacific	Open Northwest Pacific
Time	April, 2022	May-June, 2021	June-July, 2022	2012-2014		November, 2021	March-May, 2015		March-April, 2016
Size	PM_{10}	PM _{2.5}	PM_{10}	PM _{2.5}	PM _{2.5}	TSP#	PM _{2.5}	PM _{2.5}	TSP
K	2305 ± 730.0*	84.80 ± 51.00	475.0 ± 169.8	287.0 ± 48.0	91.9 ± 8.85	/	369.2 ± 225.9	149.5 ± 77.60	97.8~386.1
Ca	247.1 ± 362.3	47.00 ± 34.60	106.5 ± 105.3	605.7 ± 51.2	65.8 ± 7.26	/	139.9 ± 139.3	126.6 ± 117.9	/
Fe	228.5 ±281.5	54.90 ± 52.48	35.56 ± 99.94	194.0 ± 27.3	51.3 ± 6.73	92.0 ± 111.6	132.8 ±139.6	58.03±62.27	76.5~353.4
Mn	13.79 ± 10.88	2.05 ± 2.29	1.61 ± 6.09	12.8 ± 1.70	2.54 ± 0.29	3.12 ± 4.16	8.11±18.46	2.39±6.18	/
Ni	4.65 ± 3.44	0.97 ± 1.53	0.63 ± 1.49	3.37 ± 0.55	0.87 ± 0.13	1.50 ± 1.50	7.97±8.62	0.39±0.33	/
Cu	5.57 ± 13.00	2.16 ± 3.00	1.33 ± 2.38	29.6 ± 3.74	0.98 ± 0.16	4.37 ± 2.12	/	/	1.0~4.0
Zn	27.03 ± 28.25	7.06 ± 7.88	4.46 ± 15.88	102.0 ± 30.1	14.7 ± 2.06	11.15 ± 6.93	52.24±51.89	25.41±29.96	/
Se	1.03 ± 0.91	0.24 ± 0.32	0.34 ± 0.73	0.68 ± 0.15	0.42 ± 0.05	/	0.81±0.69	0.22±0.39	/
Cd	42.62 ± 18.20	3.44 ± 1.63	7.92 ± 1.19	0.34 ± 0.05	0.11 ± 0.01	0.08 ± 0.06	/	/	0.1~0.6
Ba	20.50 ± 20.63	5.06 ± 4.60	2.81 ± 6.83	5.69 ± 0.78	0.57 ± 0.08	/	10.72±12.17	4.91±4.15	/
Pb	11.32 ± 6.49	1.85 ± 1.88	0.72 ± 1.56	25.3 ± 4.60	4.82 ± 0.66	2.74 ± 2.27	13.77±16.10	2.50±3.50	1.9~13.1
V	7.20 ± 6.62	0.55 ± 1.20	1.56 ± 3.44	1.43 ± 0.22	1.18 ± 0.10	0.81 ± 0.77	21.35±24.03	0.38±0.79	/
As	3.12 ± 8.96	0.39 ± 0.92	0.33 ± 1.13	1.35 ± 0.23	0.60 ± 0.07	0.51 ± 0.47	1.50±3.63	0.62±1.50	/

^{*}Values with underlines indicate abnormally high concentrations, which were excluded from discussion in this study; *TSP refers to total suspended particles in the atmosphere.

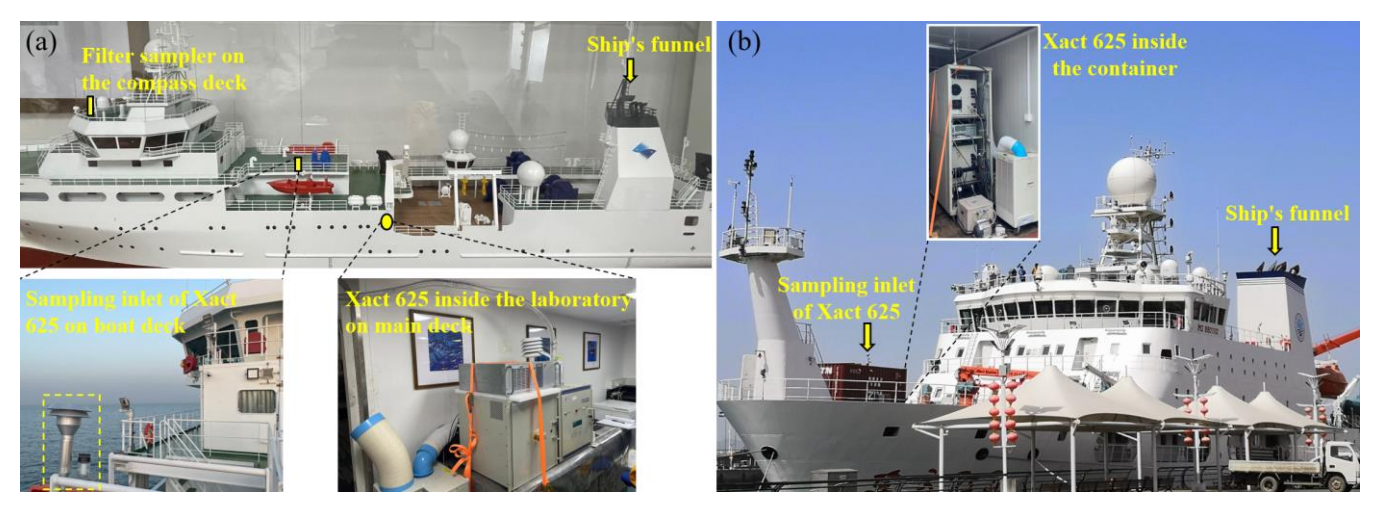


Figure S1. Instrument placement on research vessels. (a) BY cruise conducted aboard R/V *Lanhai 101*. (b) NWP1 and NWP2 cruises conducted aboard R/V *Dongfanghong 3*.

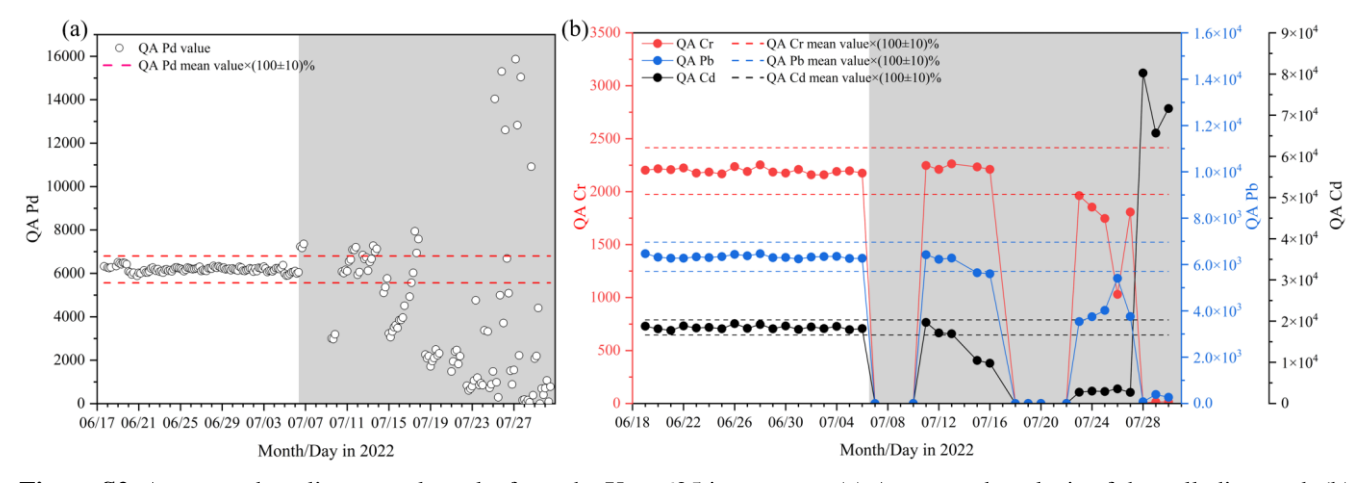


Figure S2. Automated quality control results from the Xact 625 instrument. (a) Automated analysis of the palladium rod. (b) Daily automated upscale rod check for Cr, Pb, and Cd. The two dashed lines represent ±10% deviation from the mean value, which was calculated based on measurements from June 18 to July 6, 2022.

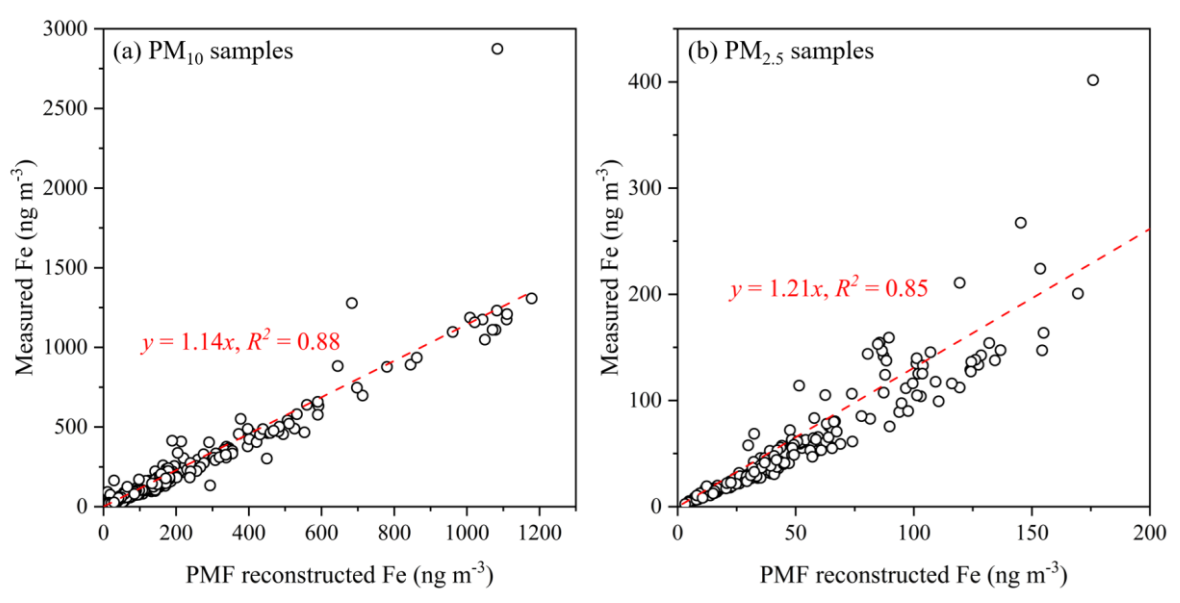


Figure S3. Scatter plots of the PMF reconstructed Fe concentrations and the measured Fe concentrations. The calculation method for PMF reconstructed Fe concentrations can be found in Text S4.

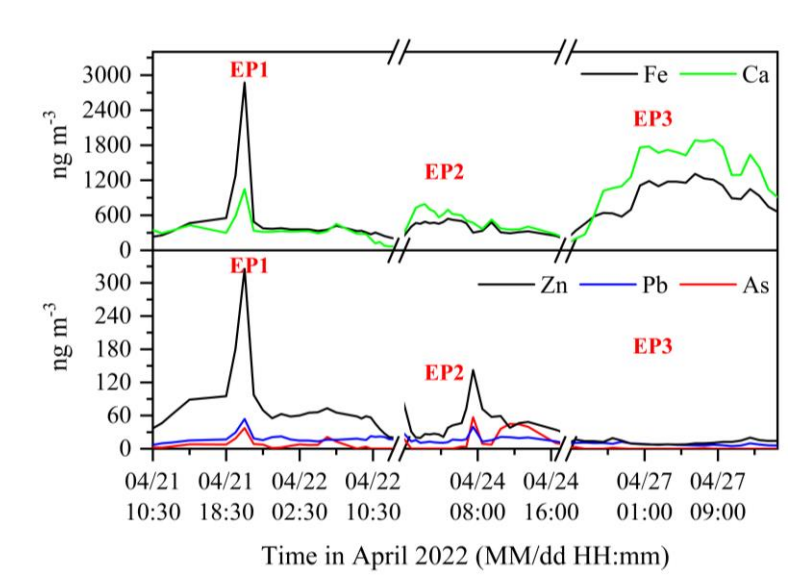


Figure S4. Concentration variations of different elements during the three high-Fe-concentration episodes. (a) Crustal elements (Ca and Fe) concentrations. (b) Pollution elements (Zn, Pb, and As) concentrations.

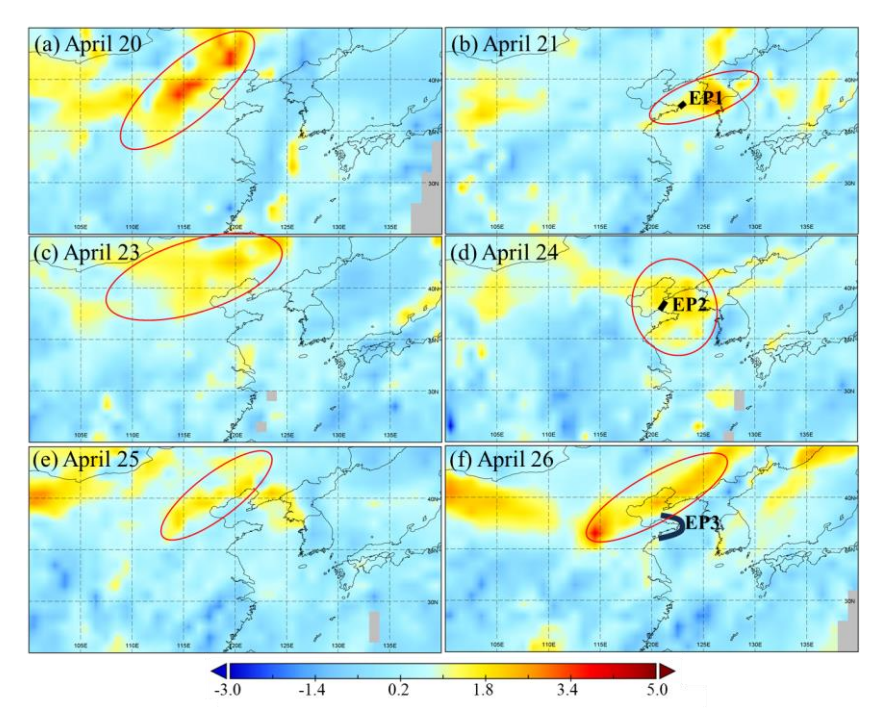


Figure S5. Spatial distributions of satellite-retrieved Absorbing Aerosol Index (AAI) during the three high-Fe-concentration episodes during BY cruise. Red ellipses highlight areas with high AAI values over upwind land regions or over the sea areas; black symbols mark sampling locations of EP1–EP3.

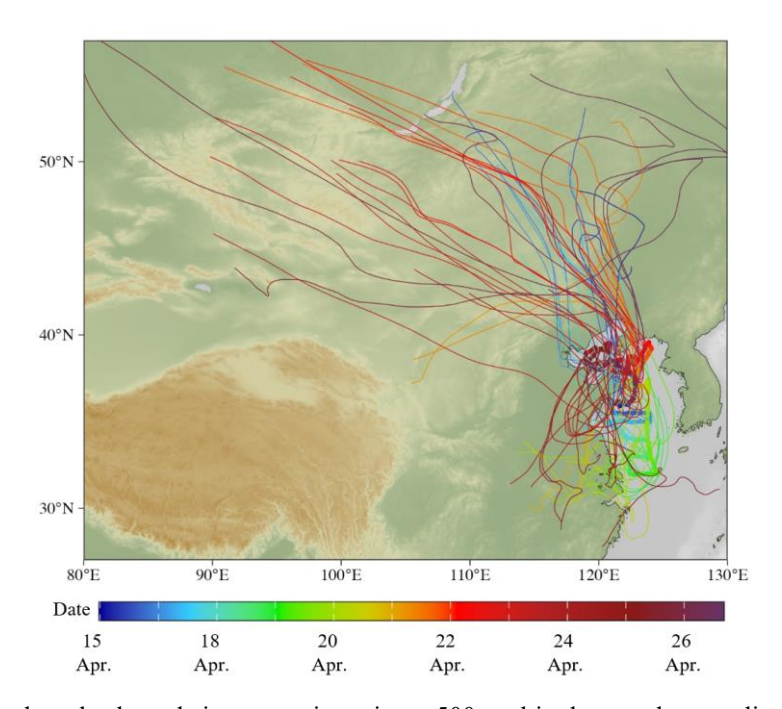


Figure S6. Seventy-two-hour backward air mass trajectories at 500 m altitude over the sampling regions during the BY cruise. The colours of the points and trajectories indicate the chronological sequence of the sampling times.



Figure S7. Photograph taken in the Yellow Sea on April 19, 2022. Vessels around the research vessel (*Lanhai 101*) are highlighted by red vertical boxes.

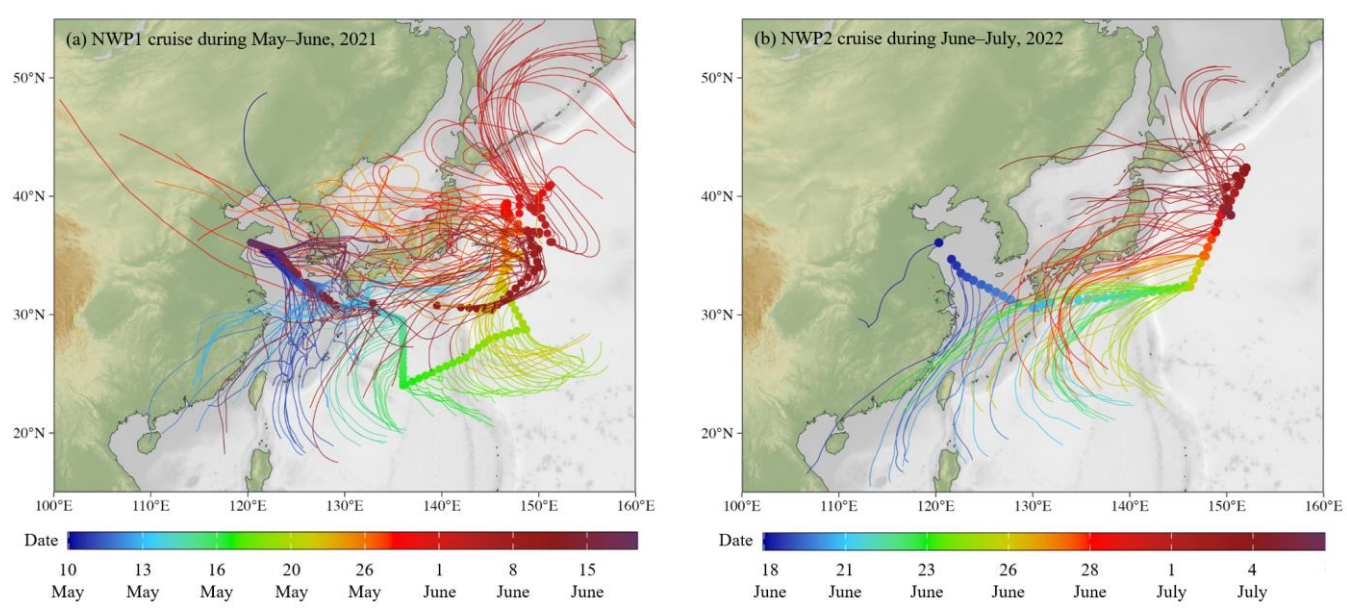


Figure S8. Seventy-two-hour backward air mass trajectories at 500 m altitude over the sampling regions during the NWP1 and NWP2 cruises. The colours of the points and trajectories indicate the chronological sequence of the sampling times.

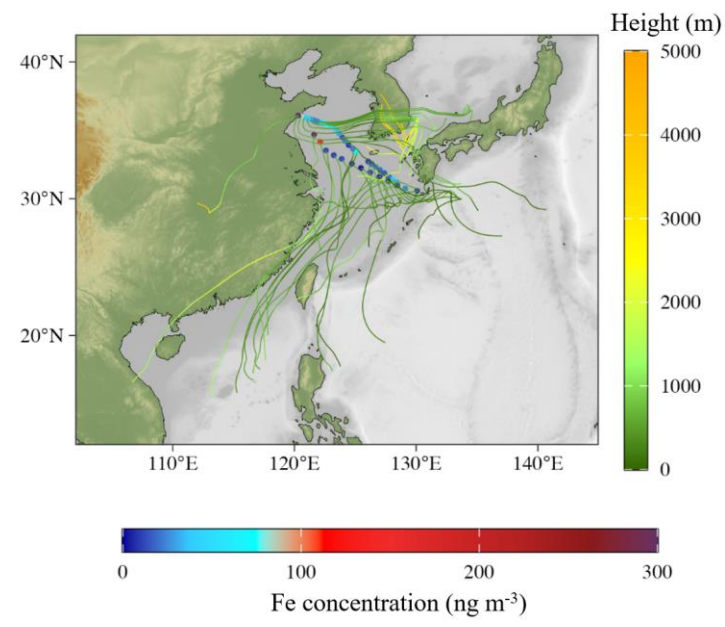


Figure S9. Seventy-two-hour backward air mass trajectories at 500 m altitude over the sampling regions during summertime in Chinese marginal Seas. The colour of the points represents the measured concentration of total Fe in the samples (ng m⁻³), while the colour of the trajectories indicates the altitude of the air masses (m).

References

- Gary, N., Rachelle, D., Steve, B., and Song, B.: EPA positive matrix factorization (PMF) 5.0 fundamentals and user guide, U.S. Environmental Protection Agency, Washington, USA, 2014. Available at:
- https://www.epa.gov/sites/default/files/2015-02/documents/pmf_5.0_user_guide.pdf (last accessed: September 22, 2025).
 - Ge, Y., Guan, W., Wong, K. H., and Zhang, R.: Spatial variability and source identification of trace elements in aerosols from Northwest Pacific Marginal Sea, Indian Ocean and South Pacific to Antarctica, Glob. Biogeochem. Cycle, 38, https://doi.org/10.1029/2024GB008235, 2024.
- Jin, T., Qi, J., Xi, Z., and Lin, X.: Impact of a dust event on the size distribution of metal elements in atmospheric aerosols at a coastal region and over the ocean, Environ. Sci., 40, 1562–1574, https://doi.org/10.13227/j.hjkx.201809012, 2019.
 - Shimada, K., Yang, X., Araki, Y., Yoshino, A., Takami, A., Chen, X., Meng, F., and Hatakeyama, S.: Concentrations of metallic elements in long-range-transported aerosols measured simultaneously at three coastal sites in China and Japan, J. Atmos. Chem., 75, 123–139, https://doi.org/10.1007/s10874-017-9366-8, 2018.
 - Zhang, H., Li, R., Dong, S., Wang, F., Zhu, Y., Meng, H., Huang, C., Ren, Y., Wang, X., Hu, X., Li, T., Peng, C., Zhang, G., Xue, L., Wang, X., and Tang, M.: Abundance and fractional solubility of aerosol iron during winter at a coastal city in Northern China: Similarities and contrasts between fine and coarse particles, J. Geophys. Res.-Atmos., 127, https://doi.org/10.1029/2021JD036070, 2022.
- Zhang, T., Liu, J., Xiang, Y., Liu, X., Zhang, J., Zhang, L., Ying, Q., Wang, Y., Wang, Y., Chen, S., Chai, F., and Zheng, M.: Quantifying anthropogenic emission of iron in marine aerosol in the Northwest Pacific with shipborne online measurements, Sci. Total Environ., 912, https://doi.org/10.1016/j.scitotenv.2023.169158, 2024.